Journal of Luminescence 261 (2023) 119906

Contents lists available at ScienceDirect

Journal of Luminescence

journal homepage: www.elsevier.com/locate/jlumin

Full Length Article

Synthesis and thermoluminescence of Ce-doped CaF_2 phosphor: Study of defect centers responsible for the TL emission by EPR analysis

Joel A. Rivera-García [a], Jessica Mosqueira-Yauri [a], T.K. Gundu Rao [a], Edwar A. Canaza-Mamani [a], Giovanni G Fiorini [b], J.F. Benavente [c], Carlos D Gonzales-Lorenzo [a], José F D Chubaci [d], Shigueo Watanabe [d], Jorge S. Ayala-Arenas [a], Nilo F. Cano [b,*]

[a] Universidad Nacional de San Agustín de Arequipa - UNSA, Peru
[b] Universidade Federal de São Paulo - UNIFESP, Instituto do Mar, Santos, SP, Brazil
[c] CIEMAT, Av. Complutense 40, E, 28040, Madrid, Spain
[d] Universidade de São Paulo, Instituto de Física, São Paulo, SP, Brazil

ARTICLE INFO

Keywords:
Calcium fluoride
Defect centers
TL
EPR

ABSTRACT

We present here the thermoluminescence (TL) properties of Ce-doped CaF_2 (CaF_2:Ce) phosphor synthesized by combustion of the precipitate formed from the addition of NH_4F to $(Ca(NO_3)_2)\cdot 4H_2O$. The structure analysis of the synthesized sample was carried out by X-ray diffraction (XRD) technique. The CaF_2:Ce phosphor shows an intense peak at about 120 °C and a low-intensity peak at 280 °C. Both peaks' thermoluminescence (TL) intensity was observed to increase with γ-dose. The kinetic parameters of TL peaks were calculated for CaF_2:Ce phosphor using the Tm-Tstop and deconvolution methods. Electron paramagnetic resonance (EPR) is utilized to identify the defect centers formed in γ-irradiated CaF_2:Ce phosphor and also to infer the defect centers involved in the TL process. The presence of two defect centers is inferred and center I has a *g*-value equal to 2.018 and is identified as an O^- ion. The O^- ion correlates with the TL peak at 120 °C. Center II with a *g*-value of 2.0057 is ascribed to a radiation-induced Fe^{3+} ion and is observed to relate to the high-temperature TL peak at 280 °C. The UV–Vis optical absorption of pure CaF_2 and Ce-doped phosphors was investigated.

1. Introduction

The development and characterization of thermoluminescent dosimeters are being widely studied. Currently, there are many materials used as thermoluminescence (TL) dosimeters in the world, of which calcium fluoride (CaF_2) has been found to be one of the most sensitive materials with very good thermoluminescent properties [1–3]. For this reason, many investigations have been carried out for the synthetic production of the material. Among fluorides, the CaF_2 crystal is an important optical material with high solubility of rare earth sensitizing and activating ions [4].

Topaksu et al. [5,6] have studied the luminescence properties of natural white fluorite irradiated by γ- and β- irradiation displaying high potential to be employed as radiation dosimeter similar to synthetic Mn-doped CaF_2 dosimeter (TLD-400).

There are many physical-chemical methods for the production of CaF_2; combustion, precipitation, and sol-gel among others [7–10]. Vasconcelos et al. [11] carried out a study of thulium-doped CaF_2 prepared by a liquid-phase synthesis method, obtaining a very radiation-sensitive material with the first TL peak at 120 °C.

Muñoz et al. [12] studied the Tm-doped CaF_2 and the first peak of the TL curve was approximately 123 °C, indicating that Eu, Cu, Ag, and Tm produce the same effect in CaF_2 samples because this peak is due to the same trap in the sample.

Salah et al. [10] synthesized CaF_2 doped with Eu, Dy, Tb, Cu, and Ag using the coprecipitation method and they obtained the same peak at approximately 125 °C to dopants Eu, Cu, and Ag. The TL sensitivity of CaF_2 was high with dopants belonging to rare earth.

Yazan et al. [13] studied the effect of Ce and Nd as co-dopants in CaF_2 samples synthesized by the solid-state reaction method. These samples present two peaks in the TL curve, the first one centered at 90° and the second one at 265 °C, the first one is 10 times more intense than

* Corresponding author..
E-mail addresses: jriveragar@unsa.edu.pe (J.A. Rivera-García), jmosqueira@unsa.edu.pe (J. Mosqueira-Yauri), jayala@unsa.edu.pe (J.S. Ayala-Arenas), nilo.cano@unifesp.br, nilocano@if.usp.br (N.F. Cano).

https://doi.org/10.1016/j.jlumin.2023.119906
Received 19 March 2023; Received in revised form 22 April 2023; Accepted 6 May 2023
Available online 9 May 2023

the second one.

Many crystalline materials, both natural and synthetic, have been widely studied for their applications in thermoluminescence (TL) radiation dosimetry. The defect centers created by ionizing radiation are responsible for TL [14]. Electron paramagnetic resonance (EPR) spectroscopy is a sensitive method used to identify and characterize these defect centers in crystalline and amorphous materials, helping to understand the mechanisms of the TL process [15]. To fully understand the nature of the centers or defects responsible for capturing electrons, thermoluminescence studies must be combined with EPR. Understanding the distribution of defects or traps in the band gap of a solid such as calcium fluoride is crucial for understanding the TL process of this material and using it in various applications.

Some authors have discussed the physical basis of the TL signal in alkaline earth fluoride crystals, such as the CaF_2 crystal, in the framework of the role of the color centers, especially the F center [16–19]. Atobe [19] has studied the changes in optical absorption bands with thermal annealing of F-centers correlated with peaks in the TL glow curve of CaF_2. However, there is no record of a correlation study between TL and EPR to identify the centers responsible for TL emission in Ce-doped CaF_2 samples.

As we can see, there are several studies of the effect of rare earth doping on the increase of the TL sensitivity of CaF_2 phosphor. However, we did not find so far, any work on Ce-doped CaF_2 phosphor using the precipitation-combustion synthesis method proposed by Vasconcelos et al. [11]. Furthermore, in order to understand better its intense TL response, we further analyzed the paramagnetic properties of the material to identify the intrinsic point defects responsible for the TL emission which is yet to be reported to the best of our knowledge.

2. Materials and methods

Undoped CaF_2, as well as CaF_2 samples doped with Ce ions (Ce = 0.1, 0.2, 0.3, 0.6, 0.8, and 1.0 mol%) were prepared by an alternative synthesis route proposed by Vasconcelos et al. [11], which consists in the combustion of a precipitate material with the main CaF_2 constituents. The calculation of the proportion between the amount of oxidizing material and fuel to have a maximum release of energy in the reaction is empirical, and established by balancing the valences of the oxidizing material (O) and fuel (C) [8,11,20]. For the fluorite, we mixed calcium nitrate tetrahydrate $(Ca(NO_3)_2)\cdot 4H_2O$ as oxidant, urea $(CO(NH_2)_2)$ as fuel [9,21], ammonium fluoride (NH_4F) as a source of fluoride, and cerium nitrate hexahydrate $(Ce(NO_3)_3\cdot 6H_2O)$ as a source of cerium in doping the CaF_2 phosphors. The used chemicals in this experiment are highly pure.

Initially, the reagents are placed in a beaker and mixed with 5 ml of distilled water. The beaker was placed on a plate maintained at approximately 42 °C and mixed using the Oxford magnetic stirrer. After reaching a gelatinous composition (precipitate formation), the precipitate was placed in the Vecstar furnace at 550 °C for combustion, where it spontaneously ignited in a few seconds. The combustion process lasted approximately 5 min.

All CaF_2 samples were ground to a very fine powder and the fine grains were used for X-ray diffraction (XRD) analysis to verify the structure of the newly synthesized material. To identify the crystalline phases of the CaF_2 sample, a Rigaku MiniFlex 600 powder diffractometer with Cu $K_{\alpha 1}$ radiation was used with a scan range of 20°–80° and a step of 0.02° with 1 s per step. The phase identification was performed using the Panalytical X'Pert HighScore Plus software.

For the study of the TL properties of the synthesized samples, pellets were fabricated by the process of pressing at room temperature and sintering. The pellets are 6.0 mm in diameter, 1.0 mm thick, and have a mass of 50 mg each.

Irradiations for TL measurements, undoped and Ce-doped CaF_2 phosphors (in pellets) were performed using a ^{60}Co source from Picker, model Gammatron, with a dose rate of 97.3 mGy/min at 10 cm from the source. On the other hand, irradiations of samples for EPR measurements were carried out with a ^{60}Co Gammacell source with a dose rate of 379.43 Gy/h. Irradiations in both sources were performed at room temperature and under electron equilibrium conditions.

TL measurements were performed on a Harshaw TL reader, model 3500, equipped with a photomultiplier for light detection. TL readings were taken from room temperature to 400 °C following a linear heating program. The heating rate of the reader is 4 °C/s in a nitrogen atmosphere. For all measurements of the TL glow curves of the CaF_2 phosphor samples, the background has been subtracted. Each point in the glow curve represents an average of five readings.

EPR spectroscopy measurements were carried out using a Freiberg Instruments Model MS5000 MiniScope X-band continuous wave EPR spectrometer. Unless otherwise specified, the EPR parameters were set: microwave frequency 9.473 GHz, microwave power 0.1 mW and 20.0 mW, modulation amplitude 0.2 mT, modulation frequency 100 kHz, sweep time 120 s, and 5 scans. All EPR measurements were performed at room temperature. Diphenyl picryl hydrazyl (DPPH) was used to calibrate the g-factors of the defect centers.

Absorbance spectra of undoped and Ce-doped CaF_2 phosphors were measured using a Shimadzu UV-1800 spectrophotometer with a wavelength range of 800 nm–200 nm.

3. Results and discussion

The formation of Ce-doped and undoped CaF_2 crystals was confirmed by studying the XRD patterns shown in Fig. 1. The appearance of sharp lines in the XRD peaks indicates the crystallinity of the prepared material. The XRD pattern of the undoped crystals matches the data of JCPDS (Joint Committee on Powder Diffraction Standards) card number 77–2093. The predominance of the face-centered cubic phase (space group: Fm3m.) of the CaF_2 sample was found. To investigate the effect of dopant on the lattice parameters was performed through Rietveld refinement of the experimental XRD data using PANalytical X'Pert HighScore Plus program. The Rietveld refinement of the CaF_2 sample is shown in Fig. 2. The position of the Bragg peaks is represented by vertical green lines and the blue line represents the difference between the

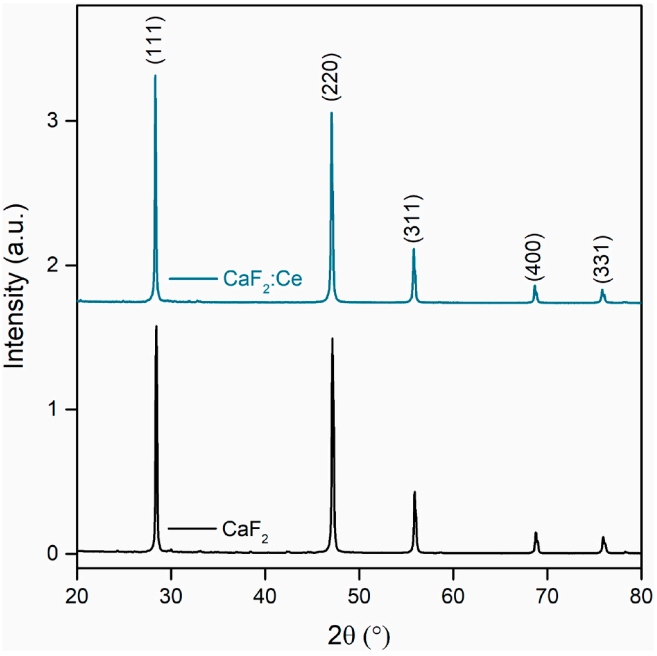

Fig. 1. XRD pattern of doped and undoped CaF_2 samples. All the reflection peaks are related to phase and matched with Miller indices (JCPDS card number 77–2093).

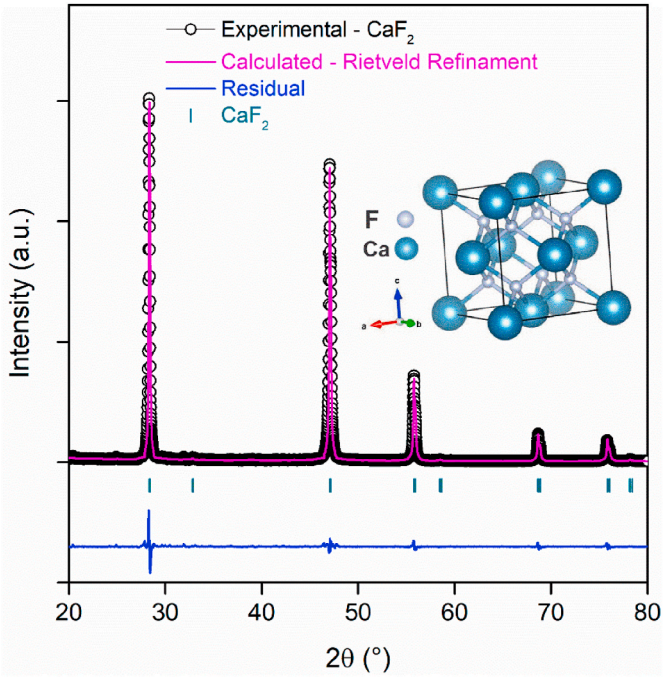

Fig. 2. XRD patterns of the CaF_2 phosphor. Experimental (open circle at black), calculated (pink solid line), residual (blue solid line), and pattern (green vertical lines are Bragg positions). The face-centered cubic crystal structure of the CaF_2 phosphor unit cell is shown in the inset of the figure.

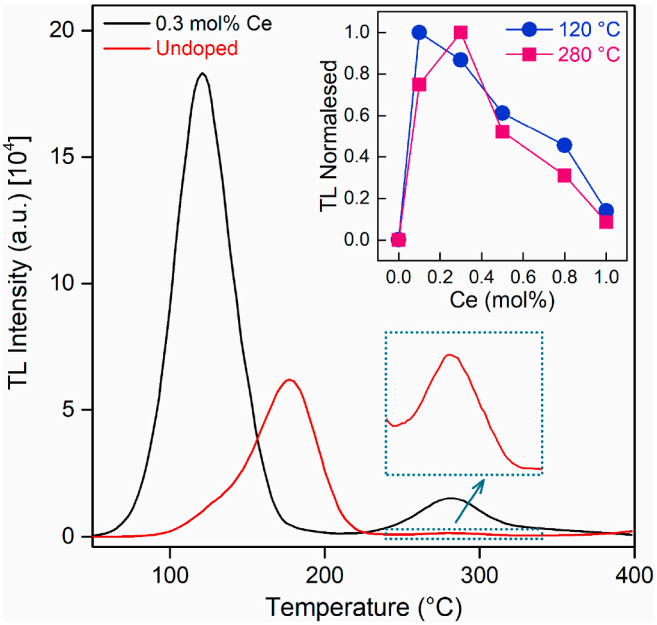

Fig. 3. TL glow curve of undoped and 0.3 mol% Ce doped CaF_2 phosphor, both irradiated with a dose of 3.0 Gy. The inset shows the normalized TL intensity of TL peaks at 120 and 280 °C as a function of Ce content.

calculated and experimental diffractograms (residual). All observed peaks satisfy the reflection conditions, suggesting the formation of a single crystalline phase for both CaF_2 samples. Therefore, the addition of the Ce dopant appears to have no effect on the XRD pattern, suggesting that Ce is incorporated into the crystal lattice without altering the periodic lattice of the synthesized material. The Scherrer equation was used to estimate the crystallite size for the diffraction peak centered at $2\theta = 47.0435°$. The refinement parameters, lattice parameters, volume, and crystallite size of the Ce-doped and undoped CaF_2 samples are listed in Table 1. The goodness-of-fit (GOF) is less than 3.74% in all cases, indicating very good consistency between the calculated profile and the experimental data.

To study the TL properties of Ce-doped CaF_2 samples calcined at 450 °C, an aliquot of each sample was irradiated with γ-rays from a ^{60}Co source with a dose of 3.0 Gy. The shape of the glow curves remained the same for all Ce concentrations. On the other hand, the peak at 180 °C of the pure sample disappears completely with Ce doping (see Fig. 3). Among the glow curves of major interest is the sample doped with 0.30 mol% Ce because it reflects a higher sensitivity for the peaks at 120 and 280 °C. Also, the inset in Fig. 3 shows that the TL intensity (normalized with the maximum intensity) of both peaks at 120 and 280 °C markedly increase with the increase in Ce content up to 0.2 and 0.3 mol%, respectively, followed by a dramatic decrease with further increase in Ce content. The TL intensity of the sample doped with 0.30 mol% Ce relative to the undoped sample is 17 times higher for the peak at 120 °C and 10 times higher for the peak at 280 °C (see the green box with dashed lines in Fig. 3), highlighting its potential application in dosimetry, mainly for the peak TL at 280 °C. Based on this observation, the sample doped with 0.3 mol% Ce was selected for further studies.

To investigate the effect of the sintering temperature of the pellets on the sensitivity of their TL response, CaF_2:Ce pellets (doped with 0.3 mol % Ce) were produced at different sintering temperatures of 450, 500, 600, and 700 °C for 2 h, and then irradiated with a γ-dose of 3.0 Gy. The CaF_2:Ce pellets show a considerable increase in TL sensitivity for the sintering temperatures of 450 and 500 °C (see Fig. 4). Analyzing the TL glow curve of these samples, the TL intensity of the peaks at 120 °C and 280 °C increased considerably for pellets sintered at 450 °C. Consequently, it is the best temperature to sinter CaF_2 pellets and obtain higher TL sensitivity of the peaks. Pellets sintered at 600 and 700 °C show a loss of TL sensitivity, mainly the first peak. In addition, for temperatures above 600 °C, there is a dislocation of the TL peak at 280 °C for lower temperatures. Sahare et al. [22] observed a similar effect with annealing temperature on the TL response in Mn, Tm and Dy doped CaF_2 samples. Therefore, pellets sintered at a temperature of 450 °C were selected for further studies. The undoped CaF_2 sample showed low sensitivity for all sintering temperatures.

The effect of γ-irradiation on the TL response of Ce-doped CaF_2

Table 1
Rietveld refinement parameters, lattice parameters, volume and crystallite size of pure CaF_2 and Ce-doped phosphors. The goodness of fit (GOF) of the refinement are also shown.

Ce concentration (mol%)	GOF			Lattice parameters		Volume	Crystallite size
	Rp	*Rwp*	χ^2	*a, b* and c (Å)	*α, β* and *γ* (°)	(Å^3)	(nm)
0.0	5.65	8.21	1.60	5.4660	90	163.31	118.7
0.1	2.87	3.77	3.33	5.4635	90	163.88	148.0
0.2	2.93	4.41	1.64	5.4629	90	163.38	147.0
0.3	5.45	7.53	1.33	5.4665	90	163.35	142.0
0.6	4.68	6.55	3.74	5.4669	90	163.40	202.1
0.8	4.90	6.74	1.73	5.4673	90	163.43	125.6
1.0	2.40	3.12	3.62	5.4652	90	163.24	115.0

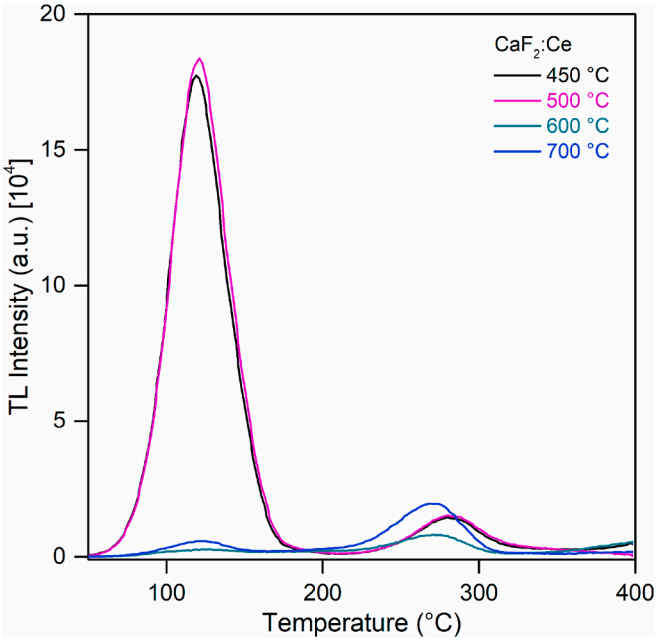

Fig. 4. TL glow curve of CaF_2:Ce pellets sintered at different temperatures.

pellets sintered at 450 °C was investigated by irradiating with γ-radiation doses in the range of 1–11 Gy. Fig. 5 shows the TL glow curve of the CaF_2:Ce pellets for different γ exposure doses, presenting a single TL glow curve with two main peaks at 120 and 280 °C. Furthermore, the intensity of the peaks of the glow curve increases with increasing γ-dose, resulting in the generation of trapping levels with γ-radiation. The inset in Fig. 5 shows that as the γ-dose increases, the intensity of the intense TL peak at approximately 120 °C increases linearly with the dose, and a second TL peak at 280 °C of low intensity grows linearly over the irradiated dose range. Since on a log-log scale, the plot is a straight line with a slope of ~1, the dependence is linear. Therefore, this sample can be used very effectively for applications in γ-radiation dosimetry.

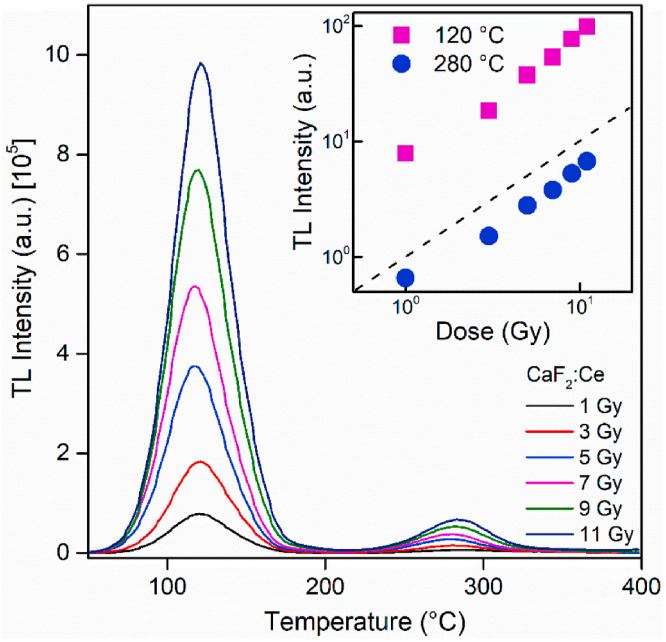

Fig. 5. TL glow curves of Ce-doped CaF_2 phosphor irradiated with γ-ray doses of 1 Gy up to 11 Gy. In the inset the TL intensity behavior as a function of γ radiation doses, the dashed lines (black) indicate linearity.

Yazan et al. [13] studied Ce and Dy's effects as co-dopants in CaF_2 samples. They found three peaks in the TL glow curve and observed the same linear behavior. Despite having obtained the materials by different synthesis techniques, the combustion of a precipitate by us and Yazan et al. [13] by the solid-state reaction method, the same TL peaks have been identified, which demonstrates the stability of the sample without depending on the type of technique used.

The TL curve for CaF_2 doped with Ce is composed of two interesting peaks, being the first more intense and more symmetrical than the others. However, a complete description of the thermoluminescent characteristics of this new material is obtained from the determination of the kinetic parameters of each TL peak, such as: activation energy, frequency factor, maximum temperature, and kinetic order. These parameters can be obtained through the analysis of the experimental TL curve using the Tm-Tstop [14] and deconvolution methods [23].

The behavior of the Tm-Tstop curve is shown in Fig. 6. It can be seen that the curve contains two regions that differ from each other. These two regions correspond to the two TL peaks observed in Fig. 6. In the first region corresponding to the Tstop temperature range from 55 to 170 °C, the presence of two subregions with very different behavior is observed, which is evidence of the superposition of at least two TL peaks. The first subregion in the interval from 55 to 120 °C with constant Tm corresponds to a TL peak with a localized energy level. The behavior of the second subregion between 125 and 170 shows an increase of the Tm value with Tstop, indicating the presence of a TL peak with an energy distribution of electron trap centers. In the second region for Tstop from 175 to 300 °C, the presence of two subregions is also observed, which evidences the superposition of at least two TL peaks for this region. The behavior of the Tm-Tstop curve for both regions and the invariance of the TL peak position at 120 and 280 °C (see Fig. 5) with dose indicate that all TL peaks of the CaF_2:Ce phosphor obey first-order kinetics (FOK), which may be due to a localized energy level or an energetic distribution of electron trap centers.

Using the preliminary analysis of the Tm-Tstop curve and applying the computerized glow curve deconvolution (CGCD) method [23], we obtain the deconvolution of the TL glow curves of the irradiated CaF_2:Ce phosphors for different γ-radiation doses. Fig. 7 shows the

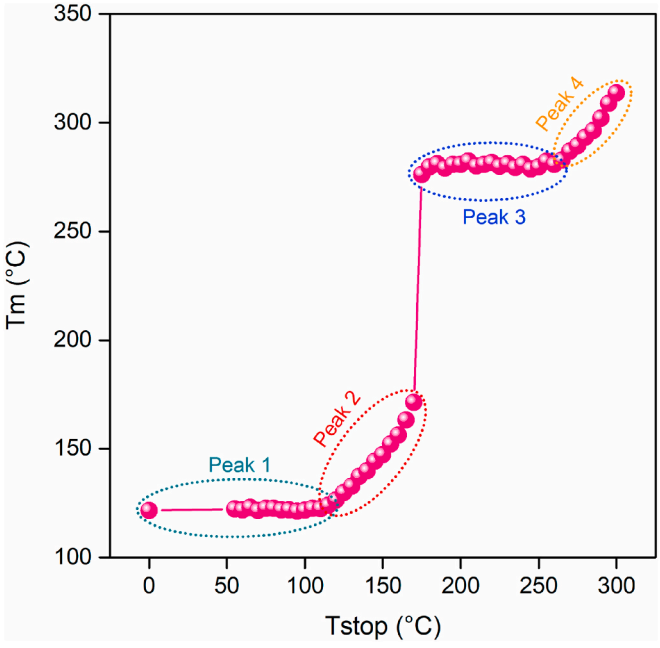

Fig. 6. Dependence of the maximum peak temperature (Tm) with the preheating temperature (Tstop). The regions of the temperature range corresponding to the four possible TL peaks of the CaF_2:Ce phosphor are indicated by dashed lines.

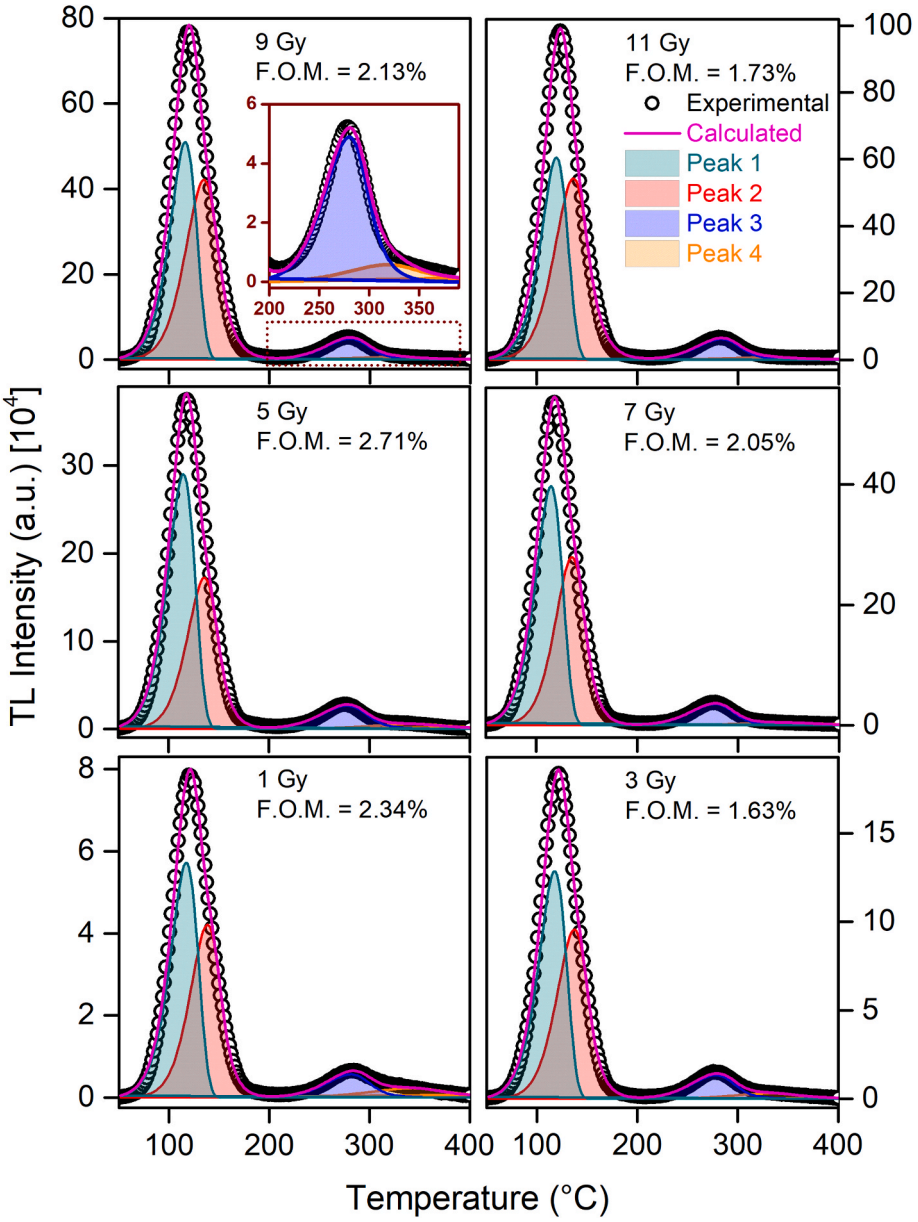

Fig. 7. Deconvoluted TL glow curves of CaF_2:Ce phosphors irradiated for different γ-doses. A good fit between the experimental glow curve (open circles at black) and the simulated glow curve (full line at pink) can be achieved by assuming the presence of four TL peaks.

deconvolution of the TL glow curves using localized trap levels and/or trap level distributions. Despite visualizing in Fig. 5 two TL peaks, the deconvolution analysis shows that the TL glow curves of the CaF_2:Ce phosphor are composed of four peaks in the region between 50 and 400 °C. All deconvolution results are optimal, both in relation to the figure of merit (FOM) value [24], with FOM values below 2.34%, as well as in the repeatability obtained. The latter quality is expressed by the low uncertainties of the kinetic parameter obtained for the six TL glow curves of the CaF_2:Ce samples (see the last row of Table 2). The first TL peak is associated with first-order kinetics (FOK) with localized trap levels. The other three TL peaks are associated with first-order kinetics (FOK) with continuous trap distribution, where each of the three traps obeys an exponential shape distribution. Table 2 shows some kinetic parameters obtained by the CGCD method, such as activation energy (E), maximum peak temperature (T), frequency factor (s), and distribution width (if applicable) for each γ-irradiation dose. The results obtained by the CGCD method are in agreement with those obtained by the Tm-Tstop method.

Fig. 8 shows the room temperature EPR spectrum of γ-irradiated (dose: 30 kGy) Ce-doped CaF_2 phosphor. It is deduced from microwave (MW) power dependence studies and thermal annealing experiments that two defect centers contribute to the observed spectrum. The centers are labeled in Fig. 8. Fig. 8 shows the spectrum recorded at low (0.1 mW) and high (20 mW) MW power levels. At low powers, center II lines are as intense as the center I lines. On the other hand, center I dominates the spectrum at high powers. Center I is characterized by a g-value equal to 2.017 and a linewidth of 18 G. This center exhibits hyperfine interaction with a nearby spin ½ nucleus and the hyperfine splitting is about 4 G.

CaF_2 is a simple alkaline earth halide and crystallizes in the space group Fm3m. Ca^{2+} ion is located in an octahedral site and is bonded to six equivalent F^- ions. F^- ions are also surrounded by six Ca^{2+} ions and the Ca^{2+} ions are situated at the corners of a regular octahedron. Each cation is symmetrically surrounded by F^- ions and vice versa.

Ca^{2+} ion in octahedral coordination in CaF_2 and the ionic radius of the ion is 1.0 Å in this six-fold coordination [25]. The dopant ion Ce^{3+} has an ionic radius of 1.01 Å in a six-fold coordination. As the ionic

Table 2
Details of activation energy (E), maximum temperature (T), frequency factors (s), order of kinetics (b) and distribution width (σ) of the TL peaks of the CaF_2:Ce phosphor obtained by the deconvolution method of the glow curves for different doses. Bottom: the average and coefficient of variation (CV).

Dose (Gy)	FOM	Peak 1: FOK (Localized)			Peak 2: FOK (Continuous)			Peak 3: FOK (Continuous)			Peak 4: FOK (Continuous)		
		E (eV)	T (°C)	s (s^{-1})	E (eV)	T (°C)	σ (eV)	s (s^{-1})	E(eV)	T (°C)	σ (eV)	s (s^{-1})	E (eV)	T (°C)	σ (eV)	s (s^{-1})
1	2.34%	0.947	117.236	$4.78{\cdot}10^{11}$	1.081	130.851	0.027	$9.32{\cdot}10^{12}$	1.357	270.811	0.035	$7.88{\cdot}10^{12}$	1.105	318.034	0.0642	$2.15{\cdot}10^{7}$
3	1.63%	0.947	117.562	$4.67{\cdot}10^{11}$	1.054	129.361	0.028	$4.76{\cdot}10^{12}$	1.333	268.055	0.032	$5.49{\cdot}10^{12}$	1.004	311.277	0.0638	$5.11{\cdot}10^{8}$
5	2.71%	0.941	114.688	$4.89{\cdot}10^{11}$	1.076	128.097	0.027	$1.03{\cdot}10^{13}$	1.266	266.660	0.033	$1.35{\cdot}10^{12}$	1.018	320.007	0.0621	$4.51{\cdot}10^{8}$
7	2.05%	0.954	114.458	$7.45{\cdot}10^{11}$	1.098	127.835	0.027	$2.03{\cdot}10^{13}$	1.339	267.068	0.031	$6.57{\cdot}10^{12}$	1.001	320.449	0.0717	$5.89{\cdot}10^{7}$
9	2.13%	0.976	116.087	$1.29{\cdot}10^{12}$	1.003	125.921	0.030	$1.36{\cdot}10^{12}$	1.359	268.926	0.037	$9.26{\cdot}10^{11}$	0.990	293.281	0.0759	$1.16{\cdot}10^{8}$
11	1.73%	0.983	117.764	$1.41{\cdot}10^{12}$	0.984	125.633	0.031	$7.77{\cdot}10^{11}$	1.377	270.672	0.037	$1.25{\cdot}10^{12}$	1.01 (9)	297.517	0.0763	$7.83{\cdot}10^{7}$
Average		0.96 (6)	116.3 (5)	–	1.05 (6)	127.9 (6)	0.03 (2)	–	1.34 (8)	268.7 (6)	0.03 (2)	–	4.34%	310 (1)	0.07 (3)	–	–
CV%		1.66%	1.15%	–	4.01%	1.42%	6.15%	–	2.63%	0.60%	6.96%	–	0.965	3.51%	8.49%	–	–

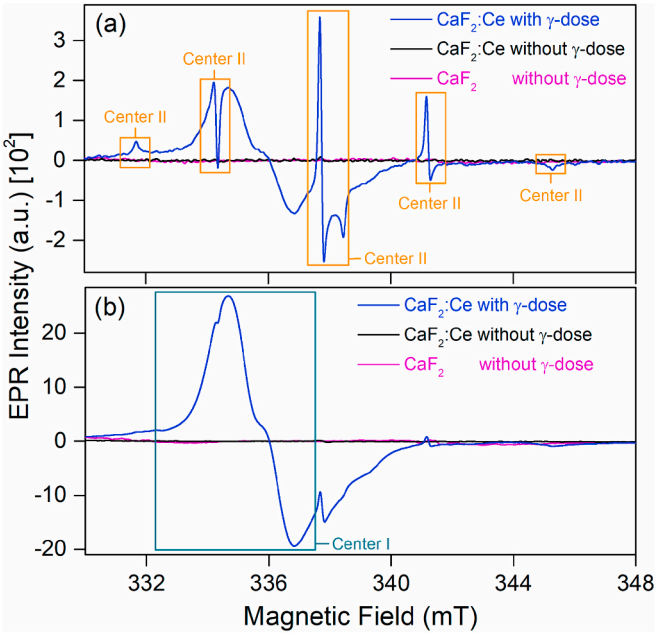

Fig. 8. Room temperature EPR spectrum of irradiated CaF_2:Ce phosphor (gamma dose: 30 kGy). The line labeled as the center I is due to an O^- ion. Center II lines are assigned to a radiation-induced Fe^{3+} ion. (a) spectrum at 0.1 mW power, (b) spectrum at 20 mW power, (c) CaF_2:Ce without γ-dose, and (d) CaF_2 pure, without γ-dose.

radius of the Ce^{3+} ion is close to that of the Ca^{2+} ion, the Ce^{3+} ion probably substitutes the Ca^{2+} ion in the CaF_2 lattice. As the trivalent Ce^{3+} ion substitutes the divalent Ca^{2+} ion, the charge balance can be obtained by F^- ions that enter the fluorite structure in interstitial fluoride cubic sites. The charge balance can also be obtained by the creation of Ca^{2+} vacancies.

The EPR line associated with center I (Fig. 8) indicates that the observed spectrum could arise from the unpaired spin's interaction with a spin ½ nucleus. The hyperfine splitting is estimated to be 4 G. The relatively large linewidth (18 G) indicates additional hyperfine interaction. Nuclear spins in close proximity can interact with the center giving rise to the unresolved hyperfine structure. ^{19}F with 100% abundance and a magnetic moment of 2.6 [26] is the possible isotope of fluorine that can interact with the unpaired spin leading this broad line.

Due to the presence of cation vacancies in the lattice, holes can be trapped to form V-centers [27]. On the other hand, electrons can be trapped at anion vacancies to form F^+ centers. Center I is tentatively attributed to an O^- ion (V-center) which is formed from an O_2^{2-} ion located adjacent to a Ca^{2+} vacancy. O_2^- ion has been observed in CaF_2 by Bill [28] and is characterized by the principal g-values $g_1 = 2.0038$, $g_2 = 2.0092$, and $g_3 = 2.0178$ at 292 K. A model of the O_2^- ion in CaF_2 lattice according to Bill is shown in Fig. 9. The O_2^- ion in CaF_2 originates from an O_2^{2-} molecule ion located in the space left by two missing mutually neighboring F^- ions. The O_2^- ion is accompanied by a neighboring cation vacancy. The O^- ion (center I) observed in the present study of CaF_2:Ce phosphor is speculated to be derived from the O_2^{2-} ion present in the CaF_2 lattice. The stability to the O^- ion is given by a neighboring Ca^{2+} vacancy.

Cation vacancies have the potential to form O^- ions by trapping holes [27]. The hole is situated in an oxygen p-orbital and the stability to the hole is provided by cation vacancies located in proximity to the O^- ion through electrostatic attraction. Positive g-shifts are expected from a hole trapped in an oxygen p-orbital. O^- ions are generally characterized by an axial g-tensor with a parallel component close to g_e (the free-spin value, 2.0023) and a perpendicular component greater than the free-spin value. There are also systems where O^- ion displays an

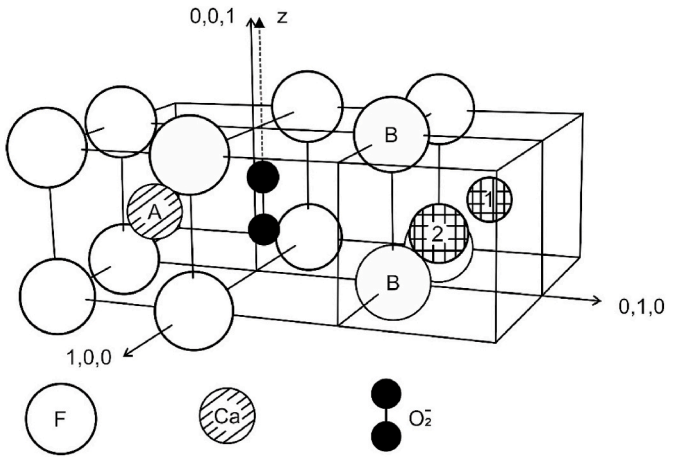

Fig. 9. CaF_2 lattice showing the model of O_2^- ion as deduced from EPR and Raman results. From H. Bill [28].

isotropic *g*-value as in $MgAl_2O_4$ studies by Ibarra et al. [29]. On the basis of optical absorption studies and EPR results, Ibarra et al. have inferred that the center in $MgAl_2O_4$ is the O^- ion. In the present study, the assignment is based on the above observations and the inference of Ibarra et al. [29].

The thermal stability of center I was studied using the pulsed thermal annealing method. This method involves heating the sample to a specific temperature and then it is kept at this temperature for 3 min. It is later cooled to room temperature for EPR experiments. The thermal annealing results of center I is shown in Fig. 10. It is seen that the center becomes unstable at about 80 °C and decays in the temperature range 80 – 270 °C. It is inferred from this behavior that center I correlates with the TL peak at 120 °C.

Thermal annealing studies show that the five lines seen in Fig. 8 (center II) arise from a single species. The center/ion associated with these lines is observable at room temperature. The *g*-value of the EPR spectrum is 2.0057 and is close to that of the free-spin value (2.0023). Among the iron group ions, the ions that exhibit a *g*-value close to the free-spin value are Mn^{2+} and Fe^{3+}. Further, the EPR spectrum of these ions is observable at room temperature. Also, both these ions display fine structure lines. The hyperfine interaction in Fe^{3+} ion is small and the hyperfine lines are rarely observed. On the other hand, Mn^{2+} ion exhibits hyperfine lines (I = 5/2). Comparing the present results with the experimental findings of Dvir and Low [30] for the Fe^{3+} ion in Beryl is noteworthy. In this case, the *g*-value is isotropic and is equal to 2.0020. Further, hyperfine lines are not observed. An examination of the relative intensities of the five lines in Beryl indicates that the extreme lines in the spectrum are due to $\pm 3/2 \rightarrow \pm 1/2$ transitions while the inner pair arises from $\pm 5/2 \rightarrow \pm 3/2$ transitions (in one specific orientation of the crystal). Similar features are observed in the present system. The maximum spectrum spread in Beryl is 1000 G. However, in the present system, it is about 136 G. The two crystal lattices are different and the observed smaller spread in CaF_2:Ce phosphor could be a result of smaller zero-field splitting as compared to the Beryl lattice. Based on these observations, the spectrum labeled as center II in Fig. 8 is tentatively assigned to a radiation-induced Fe^{3+} ion. These spectral lines are not observed in an unirradiated sample (Fig. 8). There is no intentional doping of Fe ions and as such, it is inferred that the ion originates from starting materials used in the preparation of the phosphor.

Fig. 10 shows the thermal annealing behavior of center II. It is observed that the center becomes unstable at about 160 °C and decays in the temperature range of 160 – 500 °C. Hence, it is speculated that center II may be associated with the TL peak at 285 °C.

UV–Vis absorption spectra of the CaF_2 undoped and Ce-doped were performed. All results are shown in Fig. 11. The absorbance spectra of both samples exhibit broadband in the UVC region, between 190 and 245 nm and centered at about 203 nm. A similar band was found by Pandurangappa et al. [31]. They have found an optical absorption band around 218 and 244 nm for CaF_2 nanocrystals synthesized by the co-precipitation method and hydrothermal method. They explain that these may be attributed to surface defects in nano-CaF_2 materials. That is, it is due to the large surface present in the produced nanomaterial of CaF_2. This promotes the formation of voids both on the surface and inside the agglomerating nanoparticles. These voids are responsible for the fundamental absorption in the UV wavelength range [32]. Furthermore, a small absorption bands are seen around 306 nm for the Ce-doped

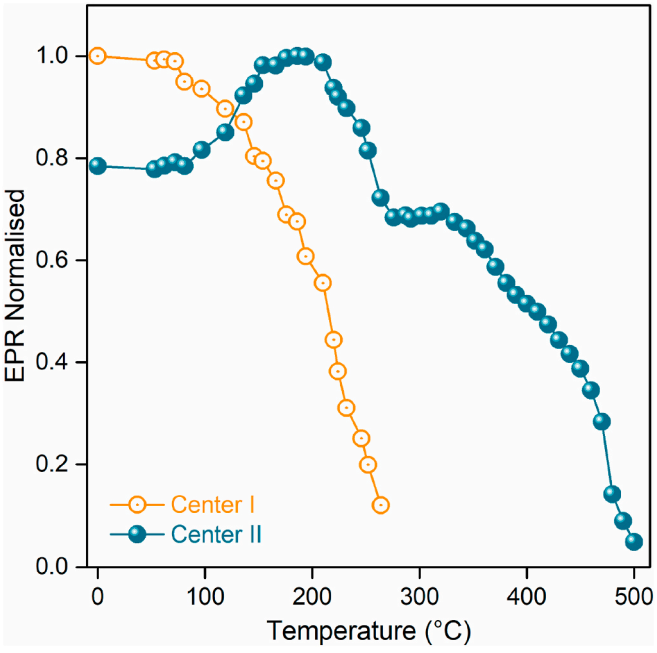

Fig. 10. Thermal annealing behavior of Center I (O^- ion) and center II (Fe^{3+} ion) in Ce-doped CaF_2 phosphor.

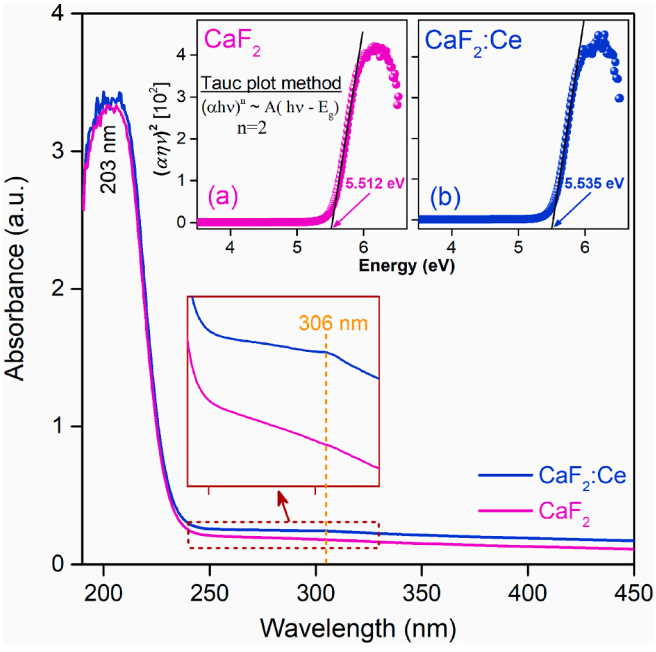

Fig. 11. UV–vis absorption spectra of undoped and Ce doped CaF_2 sample measured in the wavelength range from 190 to 450 nm. In the inset the optical band gap energy (Eg) of CaF_2 samples (a) undoped and (b) Ce-doped.

sample.

Beyond 250 nm, no significant absorption bands are observed. It shows that the CaF_2 sample, undoped and Ce-doped is transparent in the visible region with a band absorption in the UVC region. Similar results were found by Pandurangappa et al. [31], and Chauhan and Chakrabarty [33]. They have produced CaF_2 undoped and doped with Tb (3% mol). The absorption spectra show an additional band around 235 nm when CaF_2 is doped with Tb.

The optical bandgap energy (Eg) of undoped and Ce-doped CaF_2 phosphor was calculated using the Tauc ratio [34].

$$(\alpha h\nu)^n \sim (h\nu - E_g)$$

where $h\nu$ is the photon energy, α is the optical absorption coefficient near the fundamental absorption edge, and $n = 2$ for a direct transition and $n = 1/2$ for an indirect transition.

Chauhan and Chakrabarty [33] and Nakhaei et al. [35] have used a direct transition to calculate samples based on CaF_2 nanomaterials. Accordingly, a better fit was also found for a direct transition in this work. The inset of Fig. 11 (a and b) displays the curves of $(\alpha h\nu)^n$ versus $h\nu$ for direct transition where the band-gap was determined by extrapolating the straight-line section with the energy axis. The optical band gap found were 5.512 and 5.535 eV for undoped CaF_2, and Ce-doped, respectively. This small but significant variation in the bandgap as well as the presence of the small absorption band (around 306 nm) for the Ce-doped sample may be due to the effect of the rare earth dopant on the crystal structure. This effect may also be responsible for promoting the presence of luminescent centers in the crystalline structure. For both low and high-temperature traps for TL measurements as can be concluded from Fig. 3.

4. Conclusions

The XRD pattern of all the synthesized samples revealed the presence of CaF_2 crystalline phases. The sintering temperature that produces a better TL intensity is 450 °C for 2 h. The CaF_2:Ce pellets sintered at 450 °C exhibited two TL peaks at 120 and 280 °C. The TL intensity as a function of dose in log-log representation for both CaF_2:Ce TL peaks grows linearly. The kinetic parameters of the TL peaks of the phosphor glow curve such as activation energy (E), frequency factor (s), peak intensity position, and kinetic order have been estimated by Tm-Tstop and deconvolution methods, revealing four TL peaks at 116, 127, 268 and 310 °C. The superposition of the peaks at 116 and 127 °C gives rise to the first peak centered at 120 °C, and the superposition of the peaks at 268 and 310 °C gives rise to the second peak at 280 °C. Two defect centers have been identified in the CaF_2:Ce phosphor. These centers are tentatively assigned to an O^- ion and a radiation-induced Fe^{3+} ion. O^- ion (center I) correlates with the dominant TL peak at 120 °C. Fe^{3+} ion (center II) is associated with the 285 °C TL peak.

Credit author statement

J.A. Rivera-García: Data curation, Investigation. **J. Mosqueira-Yauri**: Investigation, Data curation, Methodology, Visualization, Conceptualization. **T.K. Gundu Rao**: Formal analysis, Investigation, Validation, Writing – review & editing. **E.A. anaza-Mamani**: Investigation. **G.G. Fiorini**: Investigation. **J.F. Benavente**: Investigation, Methodology, Validation. **C.D. Gonzales-Lorenzo**: Investigation. **J.F.D. Chubaci**: Investigation. S.**Watanabe**: Investigation. **J.S. Ayala-Arenas**: Funding acquisition, Investigation. **N.F. Cano**: Conceptualization, Formal analysis, Investigation, Methodology, Supervision, Validation, Visualization, Writing – original draft, Writing – review & editing.

Declaration of competing interest

The authors declare that they have no known competing financial interests or personal relationships that could have appeared to influence the work reported in this paper.

Data availability

The data that has been used is confidential.

Acknowledgments

This work was supported by "Universidad Nacional de San Agustín de Arequipa" (Process number IBAIB-02-2018-UNSA). We are grateful to Dr. B.C. Bhatt, ex Bhabha Atomic Research Center, Mumbai, India for his suggestions. The authors would like to express our thanks to Ms. E. Somessari from the Institute for Energy and Nuclear Researches (IPEN), Brazil, for kindly carrying out the gamma irradiation of the samples for the EPR measurements.

References

[1] E. Okuno, S. Watanabe, UV induced thermoluminescence on natural calcium fluoride, Health Phys. 23 (1972) 377–382.
[2] C.M. Sunta, A review of thermoluminescence of calcium fluoride, calcium sulphate and calcium carbonate, Radiat. Protect. Dosim. 8 (1984) 25–44, https://doi.org/10.1093/oxfordjournals.rpd.a083041.
[3] M. Sohrabi, F. Abbasisiar, M. Jafarizadeh, Dosimetric characteristics of natural calcium fluoride of Iran, Radiat. Protect. Dosim. 84 (1999) 277–280, https://doi.org/10.1093/oxfordjournals.rpd.a032737.
[4] G. Aldica, M. Secu, Investigations of the non-isothermal crystallization of CaF_2 nanoparticles in Sm-doped oxy-fluoride glasses, J. Non-Cryst. Solids 356 (2010) 1631–1636, https://doi.org/10.1016/j.jnoncrysol.2010.06.017.
[5] M. Topaksu, Virgilio Correcher, Javier Garcia-Guinea, Luminescence emission of natural fluorite and synthetic CaF2:Mn (TLD-400), Radiat. Phys. Chem. 119 (2016) 151–156, https://doi.org/10.1016/j.radphyschem.2015.10.002.
[6] M. Topaksu, A.N. Yazici, The thermoluminescence properties of natural CaF2 after β-irradiation, Nucl. Instrum. Methods B 264 (2007) 293–301, https://doi.org/10.1016/j.nimb.2007.09.018.
[7] J. Azorin, Preparation methods of thermoluminescent materials for dosimetric applications: an overview, Appl. Radiat. Isot. 83 (2014) 187–191, https://doi.org/10.1016/j.apradiso.2013.04.031.
[8] V.K. Asfora, V.S.M. Barros, R.J.G. Silva, D.A.A. Vasconcelos, B.S. Nobre, M. E. Yamato, H.J. Khoury, R.A. Oliveira, W.M. Azevedo, Optically stimulated luminescence of CaF_2:Tm, Radiat, Measurement 85 (2016) 73–77, https://doi.org/10.1016/j.radmeas.2015.12.012.
[9] A.S. Mukasyan, P. Epstein, P. Dinka, Solution combustion synthesis of nanomaterials, Proc. Combust. Inst. 31 (2007) 1789–1795, https://doi.org/10.1016/j.proci.2006.07.052.
[10] N. Salah, N.D. Alharbi, S.S. Habib, S.P. Lochab, Luminescence properties of CaF_2 nanostructure activated by different elements, J. Nanomater. 16 (2015) 1–7, https://doi.org/10.1155/2015/136402.
[11] D.A.A. Vasconcelos, V.S.M. Barros, H.J. Khoury, W.M. Azevedo, V.K. Asfora, P. L. Guzzo, Synthesis and thermoluminescent response of CaF_2 doped with Tm^{3+} Radiat, Measurement 71 (2014) 51–54, https://doi.org/10.1016/j.radmeas.2014.05.027.
[12] I.D. Muñoz, O. Avila, I. Gamboa-deBuen, M.E. Brandan, Evolution of the CaF_2:Tm (TLD-300) glow curve as an indicator of beam quality for low-energy photon beams, Phys. Med. Biol. 60 (2015) 2135–2144, https://doi.org/10.1088/0031-9155/60/6/2135.
[13] H. Yazan, Z.G. Portakal-Uçar, S. Akça, M. Topaksu, P.D. Townsend, N. Can, Thermoluminescence of Ce and Nd co-doped CaF_2 phosphors after beta irradiation, J. Lumin. 234 (2021), 117949, https://doi.org/10.1016/j.jlumin.2021.117949.
[14] S.W.S. McKeever, Thermoluminescence of Solids, Cambridge University Press, London, 1985.
[15] A. Marfunin, Spectroscopy: Luminescence and Radiation Centers in Minerals, Springer, Berlin, 1979.
[16] J.H. Beaumont, W. Hayes, D.L. Kirk, G.P. Summers, An investigation of trapped holes and trapped excitons in alkaline earth fluorides, Proc. R. Soc. London Ser. A 315 (1970) 69.
[17] V. Ausin, J.L. Alvarez-Rivas, Thermoluminescence and annealing of F-centres in KCl gamma irradiated at room temperature, J. Phys. Chem. 5 (1972) 82–96, https://doi.org/10.1088/0022-3719/5/1/011.
[18] D.F. Mariani, J.L. Alvarez-Rivas, Thermoluminescence in KI, KBr, NaCl and NaF crystals irradiated at room temperature, J. Phys. Chem. 11 (1978) 3499, https://doi.org/10.1088/0022-3719/11/16/019.
[19] K. Atobe, Thermoluminescence and F center annealing in alkaline earth fluoride crystals after reactor irradiation at low temperature, J. Chem. Phys. 71 (1979) 2588, https://doi.org/10.1063/1.438614.
[20] M.T.S. Medeiros, V.S.M. Barros, V.K. Asfora, H.J. Khoury, F. d'Errico, Infrared optically stimulated luminescence of rare earth doped CaF2 and co-doped with Al or Li produced by combustion synthesis, Radiat, Measurement 138 (2020), 106366, https://doi.org/10.1016/j.radmeas.2020.106366.

[21] T. Mimani, Fire synthesis: preparation of alumina products, Resonance 5 (2000) 50–57, https://doi.org/10.1007/BF02838824.
[22] P.D. Sahare, M. Singh, P. Kumar, Effect of annealing and impurity concentration on the TL characteristics of nanocrystalline Mn-doped CaF_2, Radiat. Meas. 80 (2015) 29–37, https://doi.org/10.1016/j.radmeas.2015.07.003.
[23] J.F. Benavente, J.M. Gómez-Ros, A.M. Romero, Thermoluminescence glow curve deconvolution for discrete and continuous trap distributions, Appl. Radiat. Isot. 153 (2019), 108843, https://doi.org/10.1016/j.apradiso.2019.108843.
[24] H.G. Balian, N.W. Eddy, Figure of merit (FOM), an improved criterion over the normalised chi-squared test for assessing goodness-of-fit of gamma ray spectra peaks, Nucl. Instrum. Methods 145 (1977) 389–395, https://doi.org/10.1016/0029-554X(77)90437-2.
[25] R.D. Shannon, Revised effective ionic radii and systematic studies of interatomic distances in halides and chalcogenides, Acta Crystallogr. A32 (1976) 751–767, https://doi.org/10.1107/S0567739476001551.
[26] R. C Weast, Handbook of Chemistry and Physics: A Ready-Reference Book of Chemical and Physical Data, CRC Press, 1971.
[27] M.S. Holston, J.W. McClory, N.C. Giles, L.E. Halliburton, Radiation-induced defects in $LiAlO_2$ crystals: holes trapped by lithium vacancies and their role in thermoluminescence, J. Lumin. 160 (2015) 43–49, https://doi.org/10.1016/j.jlumin.2014.11.018.
[28] H. Bill, Motional effects in the EPR spectrum of an O_2^- molecule ion in natural CaF2 crystals, Solid State Commun. 15 (1974) 911–915, https://doi.org/10.1016/0038-1098(74)90692-9.
[29] A. Ibarra, F.J. Lopez, J. Castro, V. centers, In $MgAl_2O_4$ spinels, Phys. Rev. B 44 (1991) 7256, https://doi.org/10.1103/PhysRevB.44.7256.
[30] M. Dvir, W. Low, Paramagnetic resonance and optical spectrum of iron in beryl, Phys. Rev. 119 (1960) 1587–1591, https://doi.org/10.1103/PhysRev.119.1587.
[31] B. Pandurangappa, Lakshminarasappa, B. Nagabhushana, Synthesis and characterization of CaF_2 nanocrystals, J. Alloys Compd. 489 (2010) 592–595, https://doi.org/10.1016/j.jallcom.2009.09.118.
[32] X. Zhang, Z. Quan, J. Yang, P. Yang, H. Lian, J. Lin, Solvothermal synthesis of well-dispersed MF_2 (M= Ca, Sr, Ba) nanocrystals and their optical properties, Nanotechnology 19 (2008), 075603, https://doi.org/10.1088/0957-4484/19/7/075603.
[33] S.M. Chauhan, B. Chakrabarty, Synthesis, characterization and optical properties of CaF_2 and Pb doped CaF_2 nanocrystals, Int. J. Engine Res. 3 (2014) 129–133.
[34] F. Abeles, Optical Properties of Solids, American Elsevier Publishing Co., New York, 1972.
[35] O. Nakhaei, N. Shahtahmassebi, M. Rezaeeroknabadi, M.B. Mohagheghi, Synthesis, characterization, and study of optical properties of polyvinyl alcohol/CaF_2 nanocomposite films, Sci. Iran. 19 (2012) 1979–1983, https://doi.org/10.1016/j.scient.2012.05.008.